

# Measurement of the Higgs boson decay branching ratio to charm quarks at the ILC

Y. Banda, T. Lastovicka, A. Nomerotski  
Particle Physics Department, University of Oxford  
Denys Wilkinson Building, Keble Road  
Oxford, OX1 3RH

## Abstract

We present an analysis for the measurement of the Higgs Boson branching ratio  $\text{BR}(H \rightarrow c\bar{c})$  for a light Standard Model-like Higgs boson produced at 250 GeV centre of mass energy at the International Linear Collider (ILC). The tools and technique used for the analysis are described and relative statistical uncertainties are determined.

## 1 Introduction

The measurement of the Higgs absolute branching ratios to all possible species is an important part of the ILC program, giving a precision test of the Standard Model prediction that the Higgs boson couples to each particle in proportion to its mass [1]. These measurements also discriminate between different 'Beyond the SM' scenarios [2, 3].

This study considers the Higgs decay mode to charm quarks which results in two- and four-jet final states. The expected SM Higgs boson branching ratio to charm quarks is equal to 3.0% for  $m_H = 120$  GeV and one of the main difficulties of the analysis is to separate this signal from the background of Higgs decays to b-quarks which has substantially larger Br of 68.2%. The selected decay modes exercise the tagging of charm quarks which is particularly sensitive to the vertex detector performance [4].

## 2 Event Generation and Detector Simulation

The signal events comprise of Higgs bosons decaying into charm quarks produced in Higgs-strahlung,  $e^+e^- \rightarrow ZH$  ignoring other contributing processes.

The CP-even Higgs can also be produced via WW(ZZ)-fusion processes,  $e^+e^- \rightarrow \nu\bar{\nu}W^*W^* \rightarrow \nu\bar{\nu}H$  ( $e^+e^- \rightarrow e^+e^-Z^*Z^* \rightarrow e^+e^-H$ ) as shown in Figure 1. At low centre of mass energies the Higgs-strahlung process is dominant if

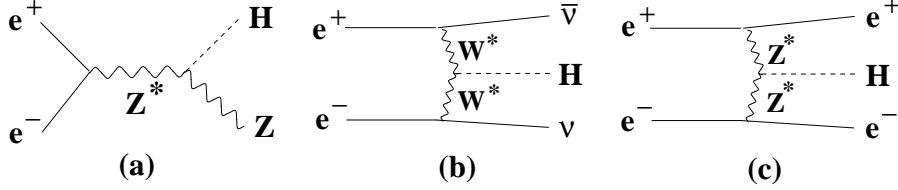


Figure 1: Higgs production in (a)Higgs-strahlung, (b) WW-fusion and (c) ZZ-fusion processes

$M_H \leq 2M_W$  due to phase space considerations. The production cross-section is shown in Figure 2 [5]. At larger CM energies ( $\sqrt{s} \geq 500$  GeV) the fusion processes start to dominate over the ZH process. The ZZ-fusion process is suppressed by one order of magnitude compared to WW-fusion due to the ratio between neutral and charged currents [6].

Both the signal and background events are produced at the centre of mass energy  $\sqrt{s} = 250$  GeV, total integrated luminosity of  $250 \text{ fb}^{-1}$  and the Higgs boson is assumed to have mass 120 GeV. The choice of energy in this analysis maximizes the cross-section value for Higgs-strahlung. Standard Model events (mainly WW, ZZ and qq pairs) and Higgs decays to other fermions other than charm quarks are considered as backgrounds. All 0, 2 and 4 fermion final states were generated using the Whizard Monte Carlo Event Generator [7]. PYTHIA [8] was used for the final state QED and QCD parton showering, fragmentation and decay to provide final-state observable particles. Photons from beamstrahlung and initial state radiation were also included in the simulations.

For this study, event samples are created conforming to the expected ILC baseline parameters of  $\pm 80\%$  electron and  $\mp 30\%$  positron polarization. About 7M events were processed through the full detector simulation, with individual events weighted to reflect the statistical sampling.

The detector response to generated events is simulated using the Geant4 toolkit [9, 10], which provides the necessary classes to describe the geometry of the detector, the transport and interaction of particles with materials and fields. A thin layer of Linear Collider specific code, SLIC [11], provides access to the Monte Carlo events, the detector geometry and the output of the detector hits. The detector parameters can be varied without having to rebuild the simulation executable binaries since the geometries are fully

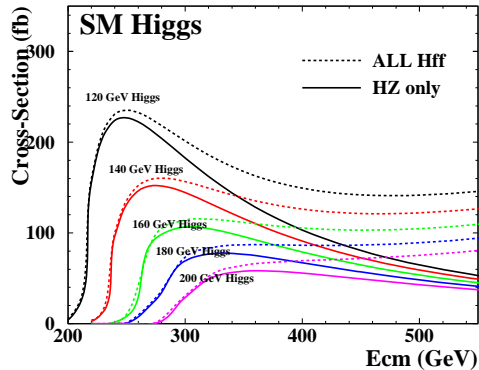


Figure 2: Production cross-section for ZH process (solid lines) and all  $Hf\bar{f}$  processes (dotted lines) for a 120-200 GeV SM Higgs as a function of the centre-of-mass energy

described at runtime. The output is in the standard LCIO format [12] so that detectors using other simulation packages can be analyzed and data generated using this system can be analyzed in other analysis frameworks.

This analysis uses the Silicon Detector (sid02) model developed by the Silicon Detector (SiD) Design Study [13]. The tracking, electromagnetic calorimetry, highly segmented hadronic calorimetry using PFA (Particle Flow Algorithm) and vertex detector are all silicon based. The SiD also incorporates a high field solenoid, iron flux return, and a muon identification system.

The vertex detector (VD) is especially important for this analysis since it relies on flavour tagging based on the lifetime information of decaying particles. The VD comprises of a central barrel system with 5 silicon pixel layers and forward and backward disk regions each with 4 pixel disks. It is enclosed within a double walled carbon fibre support. The pixels are  $20 \times 20 \mu m^2$  and the sensor thickness is taken to be  $75 \mu m$ . Sensor cut width is 8.68 mm in the innermost layer and 12.58 mm in all other layers. The sensor cut length is 125 mm for all layers. Carbon fibre cylinders support the sensors and the vertex detector is attached to the support tube with 25% material coverage support disks. For SiD, the charged track momentum resolution is expected to be better than  $\sigma(1/p_T) = 5 \times 10^{-5} (GeV/c)^{-1}$  for high momentum tracks and the impact parameter resolution will be better than  $\sigma_{r\phi} = \sigma_{rz} = 5 \oplus 10/(p \sin^{3/2} \theta) [\mu m]$ . The overall material budget for the VD per layer is 0.15% of the radiation length ( $X_0$ ). Detailed geometry description of the

detector is available at <http://lcsim.org/detectors/#sid02>.

### 3 Analysis Tools

Identification of jets is an important part of this analysis. The fragmentation products of hadronic systems are forced in  $N$  jets. The DURHAM algorithm [14] is used in the analysis and provides  $y$ -cut values that determine the separation between 1 and 2 jet cases and generally between  $N-1$  and  $N$  jet cases.

To provide the most probable kinematic configuration of the event topology a kinematic fitter (Marlin Kinfitter [15]) with four-momenta and mass constraints is used. The fitter uses the method of Lagrange multipliers to determine the most probable value for the jet four-momentum.

In order to identify primary, secondary and tertiary vertices the topological vertex finder ZVTOP is used. The algorithm is part of a vertexing package developed by the LCFI collaboration [16]. It classifies events on the number of found vertices and combines eight optimized variables for each type of event in a neural network, which is then separately trained on samples of  $b$ -,  $c$ - and light quarks. The best discriminating variables are the corrected vertex mass, secondary vertex probability, impact parameter significance of the most significant track and the number of vertices in the event. There are nine networks used with eight inputs, one hidden layer with 14 neurons and one output neuron.

Figure 3 shows the performance of the LCFI package optimized for the SiD detector. The plot shows the dependence of the purity on efficiency for the di-jet sample at  $\sqrt{s} = 500$  GeV for  $b$ -tagging,  $c$ -tagging and  $c$ -tagging with  $b$ -only background. The samples used for training of neural networks pass through the full SiD simulation and reconstruction.

The open source Fast Artificial Neural Network (FANN) package [17] is used to provide neural networks for the final event selection. The package is written in C programming language called from within a C++ wrapper.

### 4 Event Selection

The analysis signature is dependent on the  $Z$  boson decay products (charged leptons, hadrons or neutrinos). The channels studied in this analysis are the neutrino mode ( $Z$  decaying to neutrinos) and the hadronic mode ( $Z$  decaying to hadrons).

The selection of signal events is performed in three stages. The first step

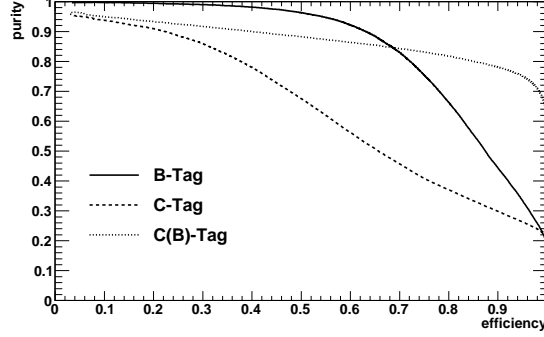


Figure 3: Purity versus Efficiency for a 500 GeV di-jet sample for b-tagging c-tagging and c-tagging with b-only background.

involves the classification of events into two channels using the number of leptons and visible energy in the event. Visible energy is defined as the sum of energies of all reconstructed particles in the event. Leptons are defined as reconstructed electrons or muons with momentum larger than 15 GeV. Figure 4 shows the distributions of the visible energy and the number of leptons for the signal (filled histogram), Higgs background (dashed line) and SM background (solid line) before any selections. The neutrino mode is selected as events with no leptons and with visible energy in the 90 to 160 GeV interval. The hadronic mode is selected as events with no leptons and the visible energy above 170 GeV.

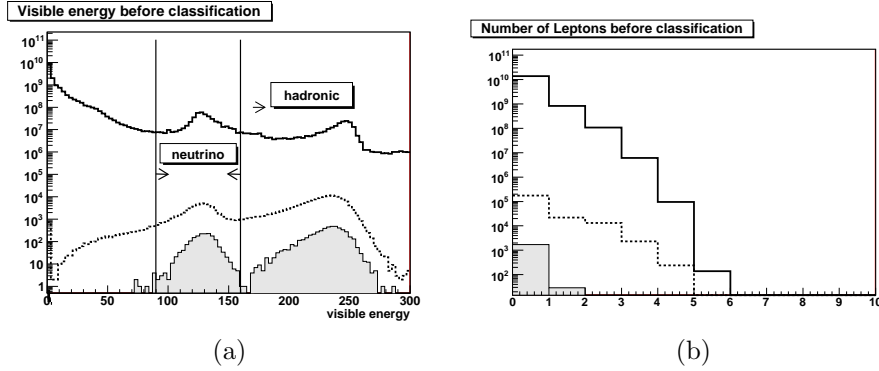


Figure 4: Visible energy (a) and the number of leptons per event (b) used for channel classification. Solid curves are SM background, dashed curves are inclusive Higgs sample and filled histograms are the signals.

The second step is a cut based selection which reduces the backgrounds in the selected channel followed by a final stage using two neural network (NN) discriminants trained on signal and two types of background samples, SM and Higgs. The remaining events after the NN selection are used for the calculation of the cross sections and branching ratios.

## 4.1 The neutrino channel

In this channel all reconstructed particles are clustered into two jets which, for the signal, are assumed to come from the Higgs boson recoiling against two neutrinos from the Z boson decay. The discrimination between the signal and background with a different number of jets is achieved by selection of the  $y_{min}$  parameter. It corresponds to the minimum y-parameter for the two jet hypothesis in the Durham algorithm. The y-parameter is defined as follows:

1. Given all pairs of particles  $\mathbf{i}, \mathbf{j}$  calculate

$$y_{ij} = \frac{2\min(E_i^2, E_j^2)(1 - \cos \theta_{ij})}{E_{vis}^2}, \quad (1)$$

where  $E_{vis}$  is the sum of the visible energies of all particles before any recombination.

2. If all  $y_{ij} > y$ -parameter stop calculation. The number of jets in the event is then defined as equal to the number of particles left.
3. Otherwise recombine the pair with the smallest  $y_{ij}$  into a single particle.
4. Finally, go back to step 1.

Therefore, in this channel the  $y_{min}$  parameter is defined as the minimum value of the y-parameter that leads to a 2-jet event. Another powerful discriminant, the reconstructed invariant mass of two hadronic jets, is expected to be consistent with the Higgs mass.

Figure 5 shows distributions of various variables used for pre-selection for the signal and backgrounds after classification. The kinematic variables used are:

- Transverse momentum of jet,  $P_T$ : The majority of SM background events are soft compared to signal events. The signal peak is expected to be at  $m_H/2$ .
- $n_{tracks}$  per event: Require more than 4 charged tracks to reject purely leptonic events

- $-\log(y_{min})$ : This variable is used to exclude fully hadronic WW (and ZZ) events which are 4-jet events mis-identified as 2-jet events. The  $-\log(y_{min})$  value is larger for the backgrounds compared to the signal.
- Thrust: This is the maximum directed momentum given by

$$T \equiv \max_{\vec{n}} \frac{\sum_i |\vec{p}_i \cdot \vec{n}|}{\sum_i |\vec{p}_i|} \quad (2)$$

Signal events are less boosted and are more spherical than the background events.

- $|\cos(\theta_{thrust})|$ : Signal events are produced more centrally in the detector while majority of the background processes have a strongly forward peaking angular distribution.
- Angle between jets: A large fraction of background events have back-to-back jets but there also backgrounds with low angular separation due to low boost. Signal events are confined to a range of angular values due to constraints coming from Z and H production.
- Di-jet invariant mass: The signal di-jet mass is required to be between 100 and 140 GeV to reject low mass hadronic systems from WW, ZZ and two-photon events
- Highest reconstructed photon energy: The signal events rarely have hard photons and this helps reject both highly energetic initial state radiation (ISR) photons and hard photons from di-jet events which occur for the background. No photon isolation is required.

The full list of selections is given in Table 1.

The background includes all SM processes. The most important are 2-fermion events, ZZ pairs decaying to neutrinos and hadrons and WW pairs where one W decays hadronically and the other W decays into a neutrino and a lepton which escapes undetected. Table 2 shows the number of events before and after pre-selection cuts.

The remaining events are categorized using the neural networks implemented in FANN [17]. The NN input variables include all the variables stated above with addition of the LCFI flavour tag outputs for both jets. Figure 6 shows the distribution of the three possible LCFI flavour tags, 'b-tag', 'c-tag' and 'c with b only background tag' for the leading jet. The first NN is trained to distinguish the SM background from the inclusive Higgs sample and to

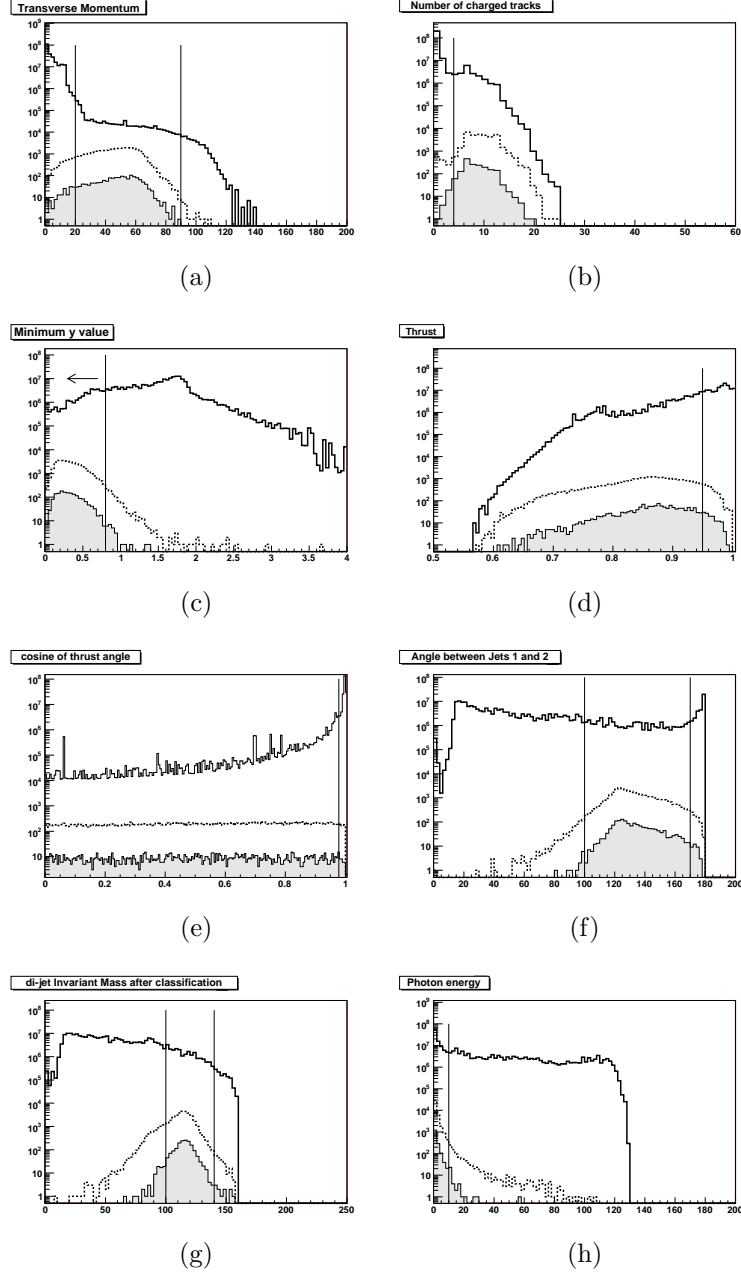


Figure 5: Distribution of pre-selection kinematic variables in the neutrino channel. Solid curves are SM background, dashed curves are inclusive Higgs sample and filled histograms is the signals.



Cut		selection	value
1.	20	$< p_T$ of jet	$< 90$ GeV
2.		number of charged tracks per event	$> 4$
3.		$-\log(y_{min})$	$< 0.8$
4.		thrust	$< 0.95$
5.		$\cos(\theta_{thrust})$	$< 0.98$
6.	$100^\circ$	$<$ angle between jets	$< 170^\circ$
7.	100 GeV	$<$ di-jet invariant mass	$< 140$ GeV
8.		Highest reconstructed photon energy	$< 10$ GeV

Table 1: Selections for the neutrino channel

Cuts	SM background	Higgs background	Signal
(i) Before Classification	9275594683	76910	2869
(0) After Classification	45936973	14294	637
(1)	18374789	13783	619
(2)	17123140	13729	618
(3)	6849256	13416	609
(4)	685329	12179	560
(5)	627113	11945	550
(6)	576422	10226	525
(7)	203292	10088	519
(8)	109057	9902	506

Table 2: Number of events before channel classification, after channel classification and after pre-selection cuts in the neutrino mode.

produce the  $NN_{SM-Higgs}$  output; and, the second NN to distinguish the signal from the Higgs background sample and to produce the  $NN_{Higgs-signal}$  output. The outputs of the trained NNs are shown in Figure 7.

Figure 8 shows scatter plots of  $NN_{Higgs-signal}$  versus  $NN_{SM-Higgs}$  for the signal and backgrounds, and also shows the number of events in different regions of  $NN_{Higgs-signal}$  and  $NN_{SM-Higgs}$  parameter space. The final event sample is required to have  $NN_{Higgs-signal} > 0.2$  and  $NN_{SM-Higgs} > 0.3$ . This cut is optimised by using different values of  $NN_{Higgs-signal}$  and  $NN_{SM-Higgs}$  and choosing a point at which the signal cross-section error is minimised (or  $S/\sqrt{B}$  ratio is maximal). The optimization is summarized in Table 3. After the final selections the sample includes 178 signal events with SM background of 140 events and Higgs background of 109 events. The signal efficiency is about 28% and the purity is 42%. The efficiency is calculated as the ratio

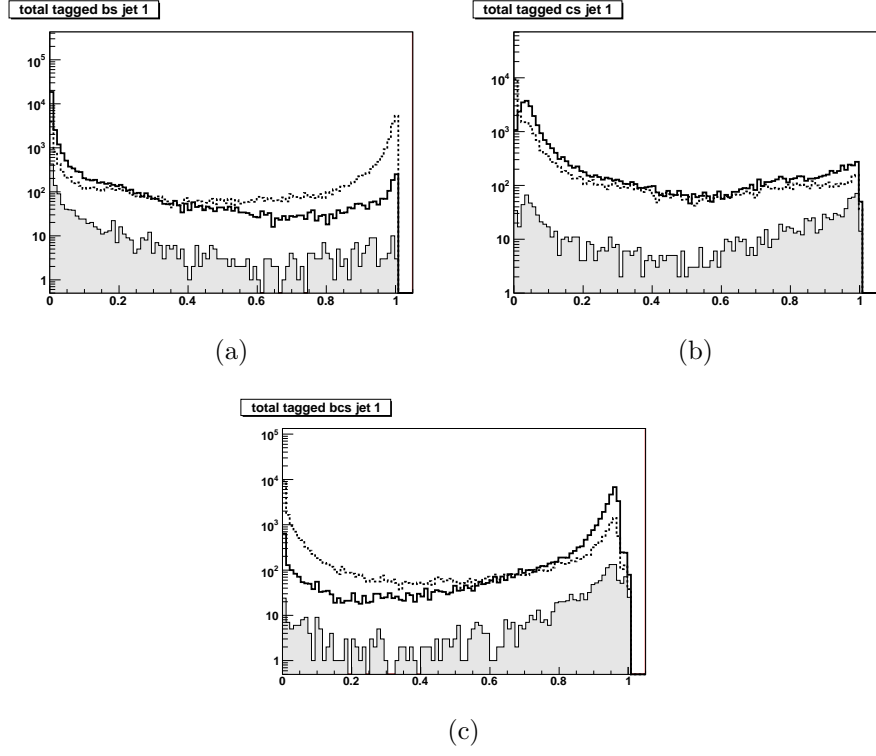


Figure 6: Neutrino channel: (a) btag; (b) ctag; (c) 'c with b background only' tag;. Solid curves are SM background, dashed curves are Higgs background sample and filled histograms are the signal.

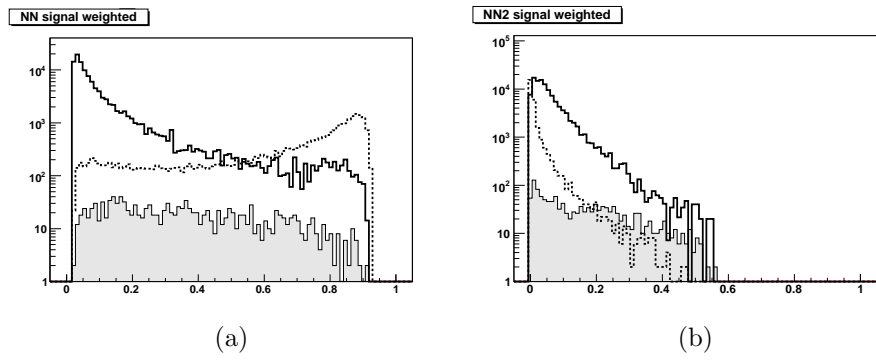


Figure 7: Neutrino channel: (a)  $NN_{SM-Higgs}$  output; (b)  $NN_{Higgs-signal}$  output. Solid curves are SM background, dashed curves are Higgs sample and filled histograms are the signals.

between the final number of signal events and the number of signal events after the classification but before the pre-selection cuts.

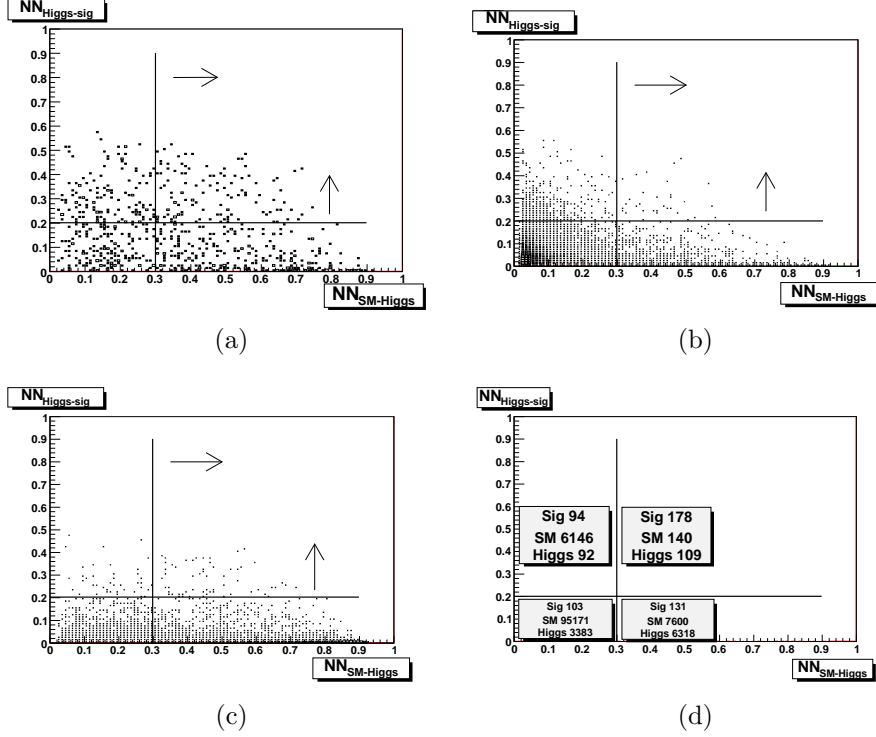


Figure 8:  $NN_{Higgs-signal}$  versus  $NN_{SM-Higgs}$  for (a) Signal, (b) Standard Model background, (c) Higgs background and (d) number of events for different NN regions

## 4.2 The hadronic channel

In the hadronic channel, events are forced to have four reconstructed jets and as in the two-jet case the  $y_{min}$  variable is chosen to differentiate from backgrounds with different numbers of jets. In this channel the  $y_{min}$  parameter is the minimum value of the y-parameter that leads to a 4-jet event configuration. For the signal, two of the jets should have di-jet invariant mass consistent with the Higgs boson and the other two having di-jet mass consistent with the Z boson.

Jet pairing is performed before kinematic fitting. For the 4-jet events we have 6 possible pairings of the jets and 3 possible associations of the 4 jets to the Z and H bosons. For the 6 possible pairings we calculate the invariant

$\text{NN}_{Higgs\text{-}signal} \downarrow$	$S/\sqrt{B}$		
$\text{NN} > 0.4$	0.8	5.4	2.7
$\text{NN} > 0.2$	1.0	<b>7.6</b>	6.0
No cut	0.3	0.7	1.0
$\text{NN}_{SM-Higgs} \rightarrow$	No cut	$\text{NN} > 0.3$	$\text{NN} > 0.6$

Table 3: Optimization of neural net cuts using  $S/\sqrt{B}$  values in the neutrino channel.

mass of each pair and compare with the masses of bosons. For each event we calculate

$$d = (m_{ij} - m_Z)^2 + (m_{kl} - m_H)^2 \quad (3)$$

The pairing that minimises  $d$  is chosen and we find on average that jets 1 and 3 are associated to the Higgs and jets 2 and 4 are associated to the Z boson, where the ranking is performed according to jet energy (jet 1 has the highest energy).

Kinematic fitting [15] is performed to improve identification of two jets from Higgs boson and two jets from Z-boson in order to reduce the combinatorial background. The kinematic fit minimizes a global chi square which is obtained from the difference between fitted and measured parameters of the kinematic variables, which are weighted by their covariance matrices. The following constraints are used for the analysis:

- $\sum_{i=0}^2 P_i = 0$
- sum of  $E = 250$  GeV
- invariant mass difference of two jet pairs is equal to difference between Higgs and Z boson masses

The main backgrounds for this channel are WW and ZZ pairs where the all bosons decay to hadrons. Figure 9 shows the Higgs and Z invariant masses before and after kinematic fitting.

For the preselection, we use kinematic cuts similar to the cuts for the neutrino channel. Figure 10 shows distributions of variables used for preselection for the signal and backgrounds after classification. The variables are as defined in Section 4.1.

Selections used for further reduction of the background are presented in Table 4. For the cuts, the jets were ordered in energy and the invariant mass and angle cuts were employed after the kinematic fitting. Table 5 shows the number of events before and after pre-selection cuts.

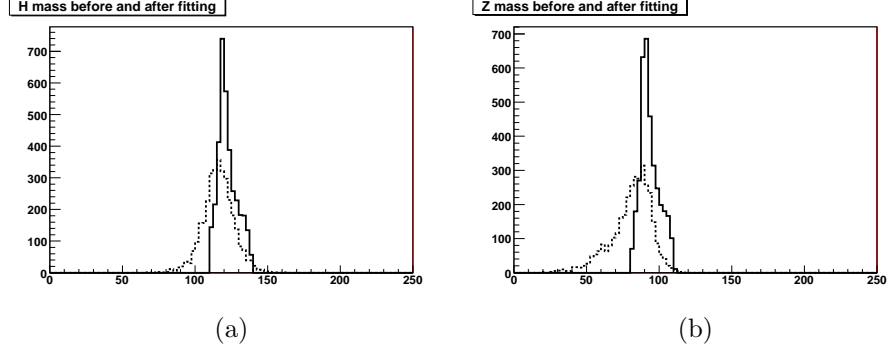


Figure 9: Higgs (a) and Z (b) invariant masses before (dashed line) and after (solid line) kinematic fitting.

For a 250 GeV centre-of-mass scenario the radiative return to the Z-peak is expected to be at around 108.6 GeV. Figure 10(i) shows the distribution of the SM reconstructed photon energy after channel classification but before any kinematic selections. We see a peak at about 125 GeV which does not correspond to the radiative return to Z-peak. The main contributions to this peak are events where a colliding  $e^+$  or  $e^-$  loses most of its energy by ISR. Figure 11(a) shows the energy of all SM background photons at the generator level after the channel classification. This distribution has two peaks at about 108 GeV and 125 GeV, which confirms that these photons originate from both Z radiative returns and direct ISR. The first peak corresponds to the radiative return to the Z-peak and the second peak corresponds to the peak observed in Figure 10(i). Figure 11(b) shows the SM reconstructed photon energy after channel classification but here all kinematic selections (1-8) are applied. Here we notice that we now have a peak at 108 GeV and no peak at around 125 GeV. We conclude that the previous selections are successful in removing photons in the other peak.

Similarly to the neutrino channel the variables above and also the three flavour tag outputs for all jets, are used in a neural network based selection employing the FANN package. Figure 12 shows the distribution of the three LCFI flavour tags, 'b-tag', 'c-tag' and 'c with b only background tag' for the first and second leading jets. The first NN is trained to distinguish the SM background from the inclusive Higgs sample producing the  $NN_{SM-Higgs}$  output, and, the second NN is trained to distinguish the signal from the Higgs background sample producing the  $NN_{Higgs-signal}$  output. The outputs of the trained NNs are shown in Figure 13.

Figure 14 shows scatter plots of  $NN_{Higgs-signal}$  versus  $NN_{SM-Higgs}$  for

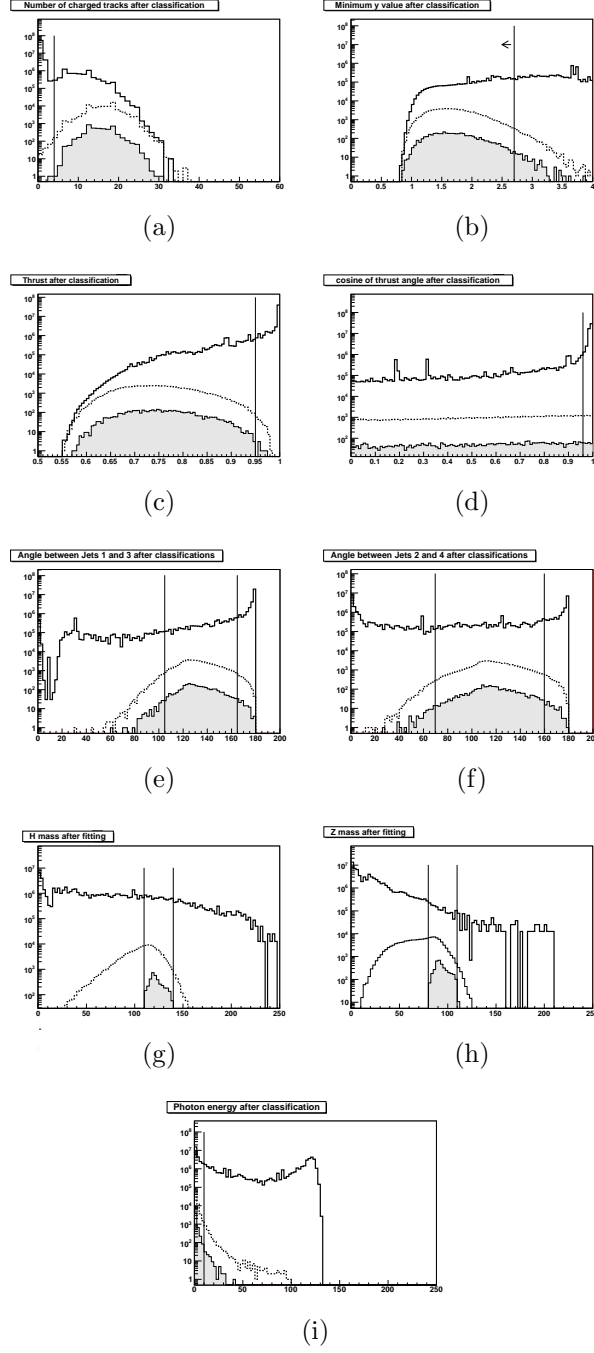


Figure 10: Distribution of pre-selection kinematic variables. Solid curves are SM background, dashed curves are Higgs background sample and filled histograms are the signal. See text for discription of variables.

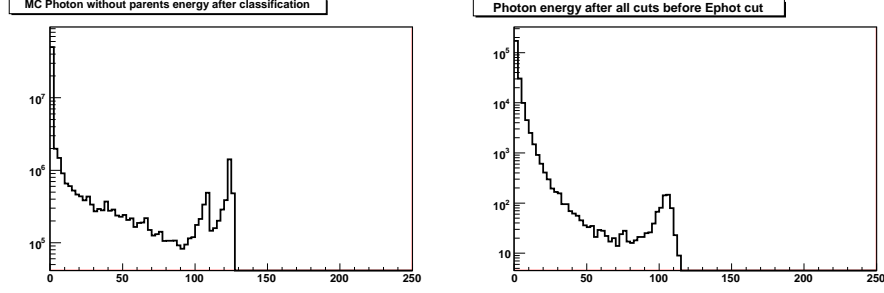


Figure 11: (a) Energy of MC photon for the Standard Model background after channel classification; (b) Energy of reconstructed photon for the Standard Model background after channel classification and kinematic selection cuts.

Cuts	selection		value
1.	number of charged tracks per event		$> 4$
2.	$-\log(y_{min})$		$< 2.7$
3.	thrust		$< 0.95$
4.	$\cos(\theta_{thrust})$		$< 0.96$
5.	$105^\circ$	$<$ angle between jet 1 and 3	$< 165^\circ$
6.	$70^\circ$	$<$ angle between jet 2 and 4	$< 160^\circ$
7.	110 GeV	$<$ invariant mass of Higgs candidate after fit	$< 140$ GeV
8.	80 GeV	$<$ invariant mass of Z candidate after fit	$< 110$ GeV
9.	Highest reconstructed photon energy		$< 10$ GeV

Table 4: Selections for the four-jet analysis.

the signal and backgrounds, and also shows the number of events in different regions of  $NN_{Higgs-signal}$  and  $NN_{SM-Higgs}$ . The final signal sample is required to have  $NN_{Higgs-signal} > 0.2$  and  $NN_{SM-Higgs} > 0.3$ . Optimisation of the NN cuts used the same method as in the neutrino channel. The optimization is summarized in Table 6. After the final selections the total number of events sample includes 407 signal events with SM background of 673 events and Higgs background of 213 events. The signal efficiency (calculated as in the neutrino channel) is about 22% and the purity is 32%.

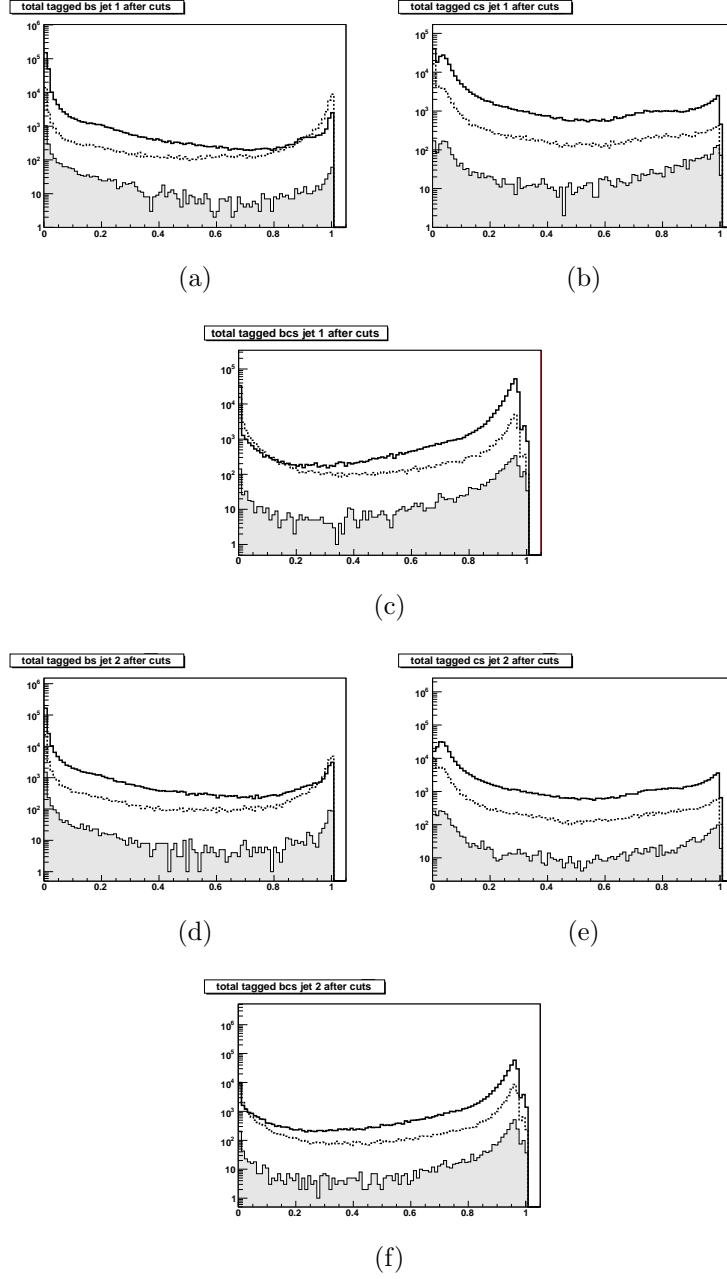


Figure 12: Hadronic channel: (a) first jet btag; (b) first jet ctags; (c) first jet 'c with b background only' tag (d) second jet btag; (e) second jet ctags; (f) second jet 'c with b background only' tag. Solid curves are SM background, dashed curves are Higgs background sample and filled histograms are the signal.



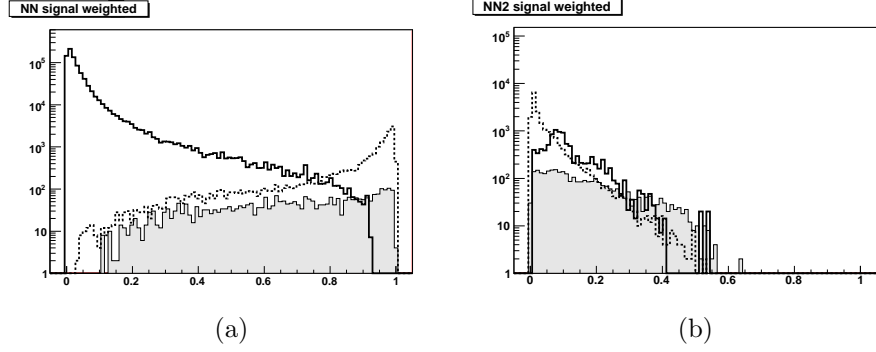


Figure 13: Hadronic channel: (a)  $NN_{SM-Higgs}$  output; (b)  $NN_{Higgs-signal}$  output. Solid curves are SM background, dashed curves are inclusive Higgs sample and filled histograms are the signals.

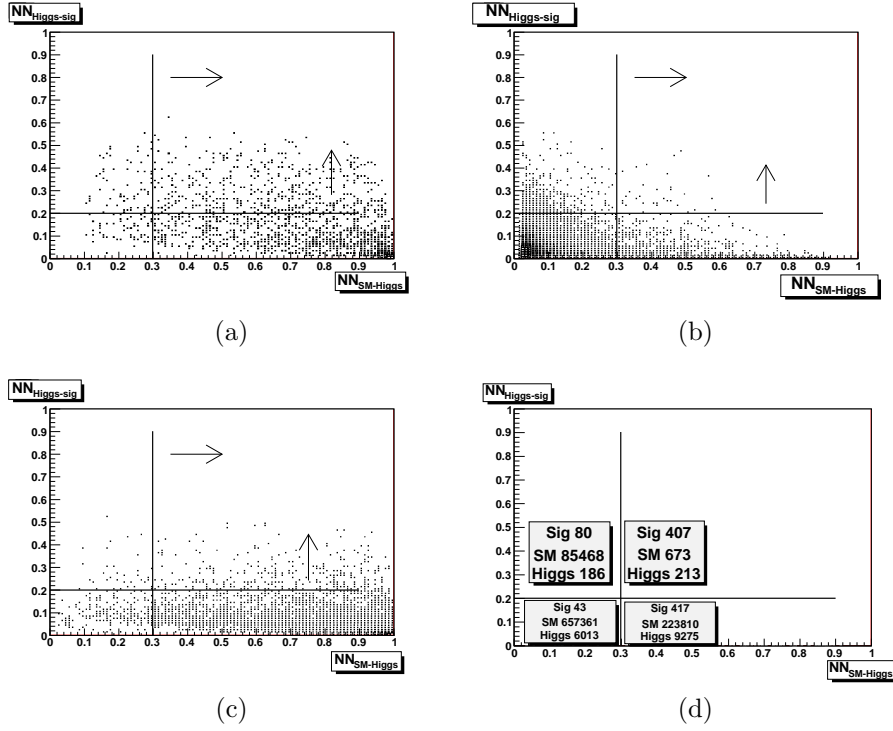


Figure 14:  $NN_{Higgs-signal}$  versus  $NN_{SM-Higgs}$  for (a) Signal, (b) Standard Model background, (c) Higgs background and (d) number of events for different NN regions.

Cuts	SM background	Higgs background	Signal
(i)Before Classification	9275594683	76910	2869
(0)After Classification	39398366	41016	1837
(1)	18601753	19954	1143
(2)	13921271	19011	1101
(3)	8737017	17743	1047
(4)	7943851	17106	1017
(5)	5871237	16262	979
(6)	4898312	16247	978
(7)	1917231	16027	966
(8)	1561432	16018	963
(9)	967312	15687	947

Table 5: Number of events before and after pre-selection cuts in the hadronic channel.

$NN_{Higgs-signal} \downarrow$	$S/\sqrt{B}$		
$NN > 0.4$	0.3	4.8	6.3
$NN > 0.2$	0.4	<b>8.7</b>	6.0
No cut	0.1	0.7	1.0
$NN_{SM-Higgs} \rightarrow$	No cut	$NN > 0.3$	$NN > 0.6$

Table 6: Optimization of neural net cuts using  $S/\sqrt{B}$  values in the hadronic channel.

## 5 Branching ratio calculation and results

The branching ratio of the Higgs boson decay to charm quarks was calculated using events that passed the final neural network selection. The calculation was done by normalising the signal cross section to the inclusive Higgs cross section,  $\sigma_{ZH} = 209 \pm 9.8$  fb, as measured in the recoil mass analysis [13].

$$BR(H \rightarrow c\bar{c}) = \frac{\sigma_{Hcc}}{\sigma_{ZH}} \quad (4)$$

The relative accuracy of the the branching ratio takes into account both the relative signal cross section uncertainty and the relative Higgs-strahlung uncertainty given as

$$\frac{\Delta BR}{BR} = \sqrt{\left(\frac{\Delta\sigma_{Hcc}}{\sigma_{Hcc}}\right)^2 + \left(\frac{\Delta\sigma_{ZH}}{\sigma_{ZH}}\right)^2} \quad (5)$$

with the relative signal cross section uncertainty calculated by

$$\frac{\Delta\sigma_{Hcc}}{\sigma_{Hcc}} = \frac{\sqrt{signal + background}}{signal} \quad (6)$$

and the cross-section is calculated as follows

$$\sigma_{Hcc} = \frac{N}{\varepsilon_{Hcc}L} \quad (7)$$

where N is the number of signal events after all selections,  $\varepsilon$  is the efficiency of signal selection and L is the total integrated luminosity.

The uncertainties in the efficiency and luminosity are considered negligible relying on simulations to determine one with sufficient precision and neglecting the systematic effects.

A summary of the results obtained for both the neutrino and hadronic channels is given in Table 7. The relative accuracy of the branching ratio in both channels is dominated by the precision of determination of the signal cross section since the uncertainty of the total Higgs-strahlung cross section is small (4.7%). The larger value of the BR uncertainty in the neutrino channel is largely due to the lower signal statistic since  $BR(Z \rightarrow \nu\bar{\nu})$  is 20.0%, and  $BR(Z \rightarrow q\bar{q})$  is 69.91%.

	Neutrino	Hadronic
Signal events	178	407
SM background events	140	673
Higgs background events	109	213
Signal efficiency %	28	22
Signal $\sigma_{Hcc}$	$6.8 \pm 0.79$ fb	$6.9 \pm 0.61$ fb
Relative uncertainty on $\sigma_{Hcc}$	11.6%	8.8%

Table 7: Branching ratio measurement results

There are two values for the relative signal cross section uncertainty, one obtained from the neutrino channel and the other from the hadronic channel. In order to find the relative uncertainty in the branching ratio we first calculate the combined signal cross section uncertainty which gives a value of 7.09%. Then using Eq. 5 we find the uncertainty in the branching ratio to be 8.5%.

## 6 Conclusion

The uncertainty of the measurement of the decay branching ratio to charm quarks for a neutral SM Higgs boson of mass 120 GeV has been studied at a

centre-of-mass of energy of  $\sqrt{s} = 250$  GeV and a total integrated luminosity of  $250 \int \text{fb}^{-1}$ . The analysis is based on full detector simulation and realistic event reconstruction. The relative uncertainties obtained are comparable to values obtained in previous studies. A good performance of flavour tagging and the use of neural networks in event selection are critical in obtaining these results. In this study we find the uncertainty on the cross section to be 11.6% in the neutrino channel and 8.8% in the hadronic channel giving a combined uncertainty on the branching ratio of 8.5%.

## References

- [1] P.W. Higgs, Broken Symmetries and the Masses of Gauge Bosons, *Phys.Rev.Lett.* 13,508 -509 (1964).
- [2] M. Carena, H.E. Haber, H.E. Logan, S. Mrenna, "Distinguishing a MSSM Higgs Boson from the SM Higgs Boson at a Linear Collider", [arXiv:hep-ph/0106116].
- [3] M. Battaglia, "Measuring Higgs Branching Ratios and telling the SM from a MSSM Higgs Boson at the  $e^+e^-$  Linear Collider", [arXiv:hep-ph/9910271].
- [4] T. Kuhl, K. Desch, "Simulation of the measurement of the hadronic branching ratios for a light Higgs boson at the ILC", LC-PHSM-2007-001.
- [5] ACFA Linear Collider Working Group, "Particle Physics Experiments at JLC", arXiv:hep-ph/0109166v1.
- [6] "Higgs Physics at LEP2", arXiv:hep-ph/9602250v1
- [7] W. Kilian, T. Ohl and J. Reuter, "WHIZARD: Simulating Multi-Particle Processes at LHC and ILC", arXiv:0708.4233 [hep-ph].
- [8] T. Sjostrand, S. Mrenna and P. Skands, "PYTHIA 6.4 physics and manual", *JHEP* **0605**, 026 (2006) [arXiv:hep-ph/0603175].
- [9] S. Agostinelli et al, "GEANT4a simulation toolkit", *Nuclear Instruments and Methods in Physics Research A* 506 (2003) 250-303.
- [10] J. Allison et al, "Geant4 developments and applications", *IEEE Transactions on Nuclear Science* 53 No. 1 (2006) 270-278.

- [11] <http://www.lcsim.org/software/slic/doxygen/html/> .
- [12] F. Gaede, T. Behnke, N. Graf and T. Johnson, LC-Note LC-TOOL-2003-053.
- [13] SiD Collaboration, "Silicon Detector Letter of Intent", <http://silicondetector.org/display/SiD/LOI> .
- [14] Yu.L. Dokshitzer In: Proc. Workshop on Jet Studies at LEP and HERA, Durham, 1990, *J. Phys G*17(1991), p.1572. //S. Catani, Yu.L. Dokshitzer, M. Olsson, G. Turnock and B.R. Webber *Phys. Lett B*269(1991), p.432
- [15] B. List, J. List, "MarlinKinfit: An Object-Oriented Kinematic Fitting Package", LC-TOOL-2009-001.
- [16] <http://hepwww.rl.ac.uk/LCFI/>; LCFI Collaboration, "LCFIVertex package: vertexing, flavour tagging and vertex charge reconstruction for the design of an ILC vertex detector", NIM paper in preparation.
- [17] <http://leenissen.dk/fann/> [leenissen.dk]